NILU: TR 4/99

NILU: TR 4/99
REFERENCE: E-99091
DATE: JULY 1999
ISBN: 82-425-1098-9

The NILU aircraft plume model: A technical description

Anne Gunn Kraabøl[1], Frode Stordal[1], Paul Konopka[2] and Svein Knudsen[1]

[1] Norwegian Institute for Air Research, N-2027 Kjeller, Norway
[2] Forschungszentrum Jülich GmbH, ICG-1, D-52425 Jülich, Germany

Norsk institutt for luftforskning
Norwegian Institute for Air Research
Postboks 100 - N-2007 Kjeller - Norway

NILU: TR 4/99

NILU: TR 4/99
REFERENCE: E-99091
DATE: JULY 1999
ISBN: 82-425-1098-9

The NILU aircraft plume model: A technical description

Anne Gunn Kraabøl[1], Frode Stordal[1], Paul Konopka[2] and Svein Knudsen[1]

[1] Norwegian Institute for Air Research, N-2027 Kjeller, Norway
[2] Forschungszentrum Jülich GmbH, ICG-1, D-52425 Jülich, Germany

Contents

The NILU aircraft plume model: A technical description

Abstract

The NILU-aircraft plume model combines the chemical and physical evolution in an aircraft plume. It describes the plume within a day after emissions. This report gives a detailed description of the plume dispersion, the diffusion within the different layers of the plume and the tropospheric chemistry scheme used in the model.

1 Introduction

The NILU-aircraft plume model describes the dilution of the emitted species due to plume expansion, diffusion within the plume and chemical transformations in the plume. It is based on a model originally developed at NILU to study dispersion and chemistry of plumes in the boundary layer (Grønskei et al., 1993). The model has been further developed to describe conditions in the free troposphere by including a chemistry scheme for this regions and a dispersion approximation for aircraft plumes at cruising altitude (Konopka, 1995; Schumann et al., 1995). In addition, a model version also includes a chemistry scheme for the stratosphere. The plume is divided into several cross-sectional layers in order to resolve the inhomogeneous distribution in the plume, and mixing within the plume is described as diffusion in the model (Figure 1). The model thus consists of the following modules: Calculation of the horizontal and vertical dispersion of the plume, calculation of diffusion between the layers, and calculation of a detailed photo-chemistry for the free troposphere or the stratosphere in the layers.

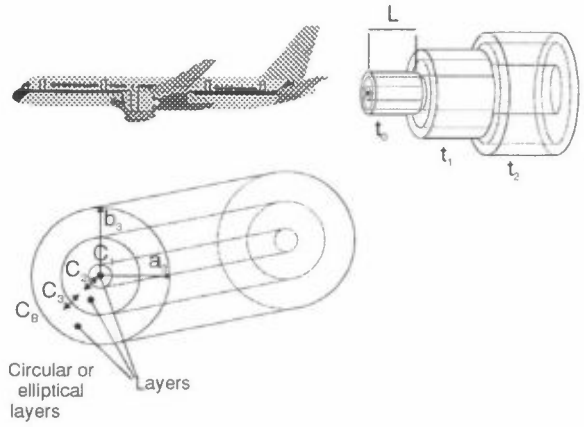

Figure 1: The NILU-aircraft plume model. The upper part shows the plume from a side view at different times (t_0, t_1,....t_n). The lower panel shows a cross section of the plume. C_1 to C_3 indicate the concentration in the plume. (Only three of the eight layers are shown.) The arrows indicate diffusion between the layers in the plume.

The tropospheric version was applied within the Pollution of Aircraft Emissions within the North Atlantic Flight Corridor (POLINAT) project, where the main objective was to study the chemical conversion of the emitted NO_x to reservoir species and the ozone evolution in the plume (Kraabøl et al., 1997). The stratospheric version has been used within the POLINAT 2 project, where the main aim was to study the chlorine activation in connection with particles that might form in the plume (Kraabøl et al., 1999). In this report, only the tropsopheric chemistry scheme is described. The stratospheric chemistry scheme is documented in Fløisand (1999).

2 Dispersion of the plume

The plume behind an aircraft can be described in three regimes: the jet regime, the vortex regime and the dispersion regime. The present model describes the two latter, as calculations start at the end of the jet regime where the flow times are between 1 and 10 s (Hoshizaki et al., 1975). During the vortex regime, the exhaust gases are efficiently trapped by two trailing vortex pair. We assume that both at the end of the jet as well as during the vortex regime, the aircraft wakes can be replaced by only one plume with an effective circular cross section A. The notation $A(t) = \pi\sigma(t)^2$ with $\sigma(t = 4\ s) = \sigma_{jet}$ and $\sigma(4 < t < 124\ s) = \sigma_{vor}(t)$ is used, where σ denotes the standard deviation of a passive tracer with Gaussian profile. Here, σ_{vor} is a linear function of the time, t.

At the beginning of the dispersion regime, which starts after about 2 minutes (min), the vortex pair breaks down. This phase, which lasts for about 1 min, is characterised by a transition of the wake-growth from aircraft- to atmospheric-induced dispersion connected with a rather sudden mixing of the exhaust gases with the surroundings. We assume that the plume's cross section changes from circular to elliptical during this process, with the horizontal and vertical widths $\sigma_h(t)$ and $\sigma_v(t)$, respectively.

The atmospheric-induced plume dispersion (sometimes called diffusion regime) is dominated by atmospheric turbulence. Here, we describe the plume dynamics in a frame of reference moving with the mean velocity of the plume determined at the centre of the plume cross section. Furthermore, we assume that the plume dispersion can be divided in to N periods $t_0 < t_1 < \ldots < t_N = t$, during which all the parameters of dispersion are held constant. Note that these intervals do not correspond to the time steps of the plume model.

In each time interval $\alpha = 1,\ldots,N$, the plume is distorted by both the wind shear, s_α perpendicular to the plume's axis, and the turbulent diffusion with an anisotropic diffusivity tensor **D**. This tensor is described in terms of horizontal, vertical, and skewed components $D_{h\alpha}$, $D_{v\alpha}$, and $D_{s\alpha}$ with

$$D_{h_\alpha}, D_{v_\alpha} > 0, \quad D_{s_\alpha}^2 < D_{h_\alpha} D_{v_\alpha}. \tag{1}$$

If the plume concentration at the beginning of the diffusion regime can be approximated by a Gaussian distribution, the analytical solutions of the corresponding atmospheric diffusion equation can be derived (Konopka et al.,

1995). These solutions can be written as Gaussian functions with a positive-definite and symmetric variance matrix

$$\hat{\boldsymbol{\sigma}}(t)=\begin{pmatrix}\hat{\sigma}_h(t) & \hat{\sigma}_s(t)\\ \hat{\sigma}_s(t) & \hat{\sigma}_v(t)\end{pmatrix}. \tag{2}$$

After $N + 1$ steps of dispersion, the components of this matrix are given recursively, i.e.

$$\begin{aligned}&\hat{\sigma}_h(t)=\sigma_h^2(t)=\sigma_{h_N}^2,\ \hat{\sigma}_s(t)=\hat{\sigma}_{s_N},\\ &\hat{\sigma}_v(t)=\sigma_v^2(t)=\sigma_{v_N}^2,\end{aligned} \tag{3}$$

with

$$\begin{aligned}\sigma_{h_{\alpha+1}}^2 &= \frac{2}{3}s_\alpha^2 D_{v_\alpha}\Delta t^3+\left(2s_\alpha D_{s_\alpha}+s_\alpha^2\sigma_{v_\alpha}^2\right)\Delta t^2+\\ &\quad 2\left(s_\alpha\hat{\sigma}_{s_\alpha}+D_{h_\alpha}\right)\Delta t+\sigma_{h_\alpha}^2,\\ \hat{\sigma}_{s_{\alpha+1}} &= s_\alpha D_{v_\alpha}\Delta t^2+\left(s_\alpha\sigma_{v_\alpha}^2+2D_{s_\alpha}\right)\Delta t+\hat{\sigma}_{s_\alpha},\\ \sigma_{v_{\alpha+1}}^2 &= 2D_{v_\alpha}\Delta t+\sigma_{v_\alpha}^2,\\ \Delta t &:= t_{\alpha+1}-t_\alpha,\ \alpha=1,\ldots,N-1\end{aligned} \tag{4}$$

where σ_{h0} and σ_{v0} are horizontal and vertical standard deviations at the beginning of the dispersion regime, respectively. Furthermore, we assume that the skewed standard deviation, $\hat{\sigma}_{s_0}=0$. This implies that during the aircraft-dominated dispersion the plume cross section can be viewed as an ellipse with vertical and horizontal principal axes.

In the dispersion regime, the wind shear and the skewed diffusion component cause both a rotation and a deformation of the plume. The rotation of the plume has no impact on the chemical conversions or the diffusion within the plume. It is important to take the skewed deformation into account, since it has an impact on the cross-sectional area of the plume. Instead of describing the plume size in terms of σ_h, σ_v, and σ_s, it is more convenient to describe the plume in terms of a minor and a major axis. These axes follow the plume rotation and take into account the off diagonal diffusion and the wind shear.

The elliptic cross section of the plume is thereby described in terms of the principal axes. Using these axes as a new frame of co-ordinates, the variance matrix, $\hat{\boldsymbol{\sigma}}$, is simplified to a diagonal form

$$\hat{\boldsymbol{\sigma}}(t)=\begin{pmatrix}\sigma^2{}_{minor}(t) & 0\\ 0 & \sigma_{major}^2(t)\end{pmatrix}, \tag{5}$$

with

$$\sigma_{minor}^2 = \frac{1}{2}\left(\hat{\sigma}_h + \hat{\sigma}_v - \sqrt{\Delta}\right) \tag{6}$$

$$\sigma_{major}^2 = \frac{1}{2}\left(\hat{\sigma}_h + \hat{\sigma}_v - \sqrt{\Delta}\right) \tag{7}$$

and

$$\Delta = \left(\hat{\sigma}_h - \hat{\sigma}_v\right)^2 + 4\hat{\sigma}_s^2 \,. \tag{8}$$

Here, σ_{minor} and σ_{major} denote the shorter and larger principal axis, respectively. Note, that the effective cross section of the plume is defined by

$$A = \pi\sigma_{minor}\sigma_{major} = \pi\left(\sigma_h^2\sigma_v^2 - \hat{\sigma}_s^2\right)^{1/2} \tag{9}$$

To describe the dispersion of the plume in all regimes, the notation σ_{major} and σ_{minor} is used. In particular, σ_{major} and σ_{minor} coincide with σ_{vor} during the vortex regime and correspond to σ_h and σ_v in the transition phase between the vortex regime and the atmospheric induced dispersion. The rate of dispersion during the different regimes is given in section 2.1.

In order to take into account the inhomogeneous concentration profiles, the plume is divided into 8 circular or elliptical cross sectional layers perpendicular to the plume centreline (Figure 1 lower panel, only three layers are shown). The axes from the plume centre to the boundary of the different layers are given as

$$a_i = f_i\sigma_{major}, \quad b_i = f_i\sigma_{minor} \tag{10}$$

where $f_i = \frac{3}{8}i$, i = 1,...,8. L is the length of the plume, and is set equal to the distance the aircraft covers during 1 s (Figure 1, upper panel). Consequently, the plume is divided into cylindrical layers parallel to the plume centreline. The volume of each cylinder with a length L can be expressed as

$$V_i = \pi L\left(a_i b_i - a_{i-1}b_{i-1}\right), \quad a_0 = b_0 = 0 \,. \tag{11}$$

The volume of the cylindrical layers increase outwards in the plume, since the radial distance between the layers is constant.

When the plume expands, the boundary of the layers are redefined and the grid resolution is adjusted. The boundaries are therefore always in accordance with equation (10, with current values of σ_{major} and σ_{minor}. This redefinition keeps the plume within the defined 8 layers. It is important to stress that this only constitutes a redefinition of the grid leading to dilution in the plume, and does not involve diffusion between the layers (section 3).

When the boundary of the layers are redefined, the concentrations of the chemical species are redistributed by volume weighting:

$$c_{k,i}(t+dt) = \frac{c_{k,i}(t)\cdot\left(V_i - \hat{V}_{i-1}\right) + c_{k,i+1}(t)\cdot\left(\hat{V}_i - V_i\right)}{\hat{V}_i - \hat{V}_{i-1}}, \qquad (12)$$

where $c_{k,i}$ is the concentration in layer i for species k, V_i is the volume at the time t for layer i, and $\hat{V}_i$ is the volume at $t = t + dt$ for layer i (Figure 2). Note that $\hat{V}_0 = 0$ and c_9 is set equal to the background concentration.

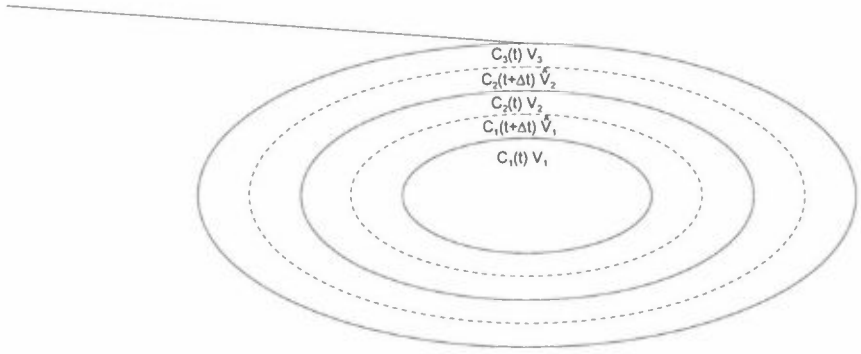

Figure 2: The cross section of the plume. The solid lines are the boundaries at time t, *while the dotted lines are the boundaries at time* t = t + dt.

2.1 Dispersion parameters

In this section, the rates of plume dispersion in the different regimes are described. At the start of the vortex regime, $\sigma_{vor}(t_0)$ is set equal to 6 m. This leads to plume mixing ratios of the emitted species, which are in accordance with the entrainment rates typically used in the box models describing the jet regime (Kärcher, 1995; Kärcher et al., 1996).

The estimates of $\sigma_{vor}(t)$ and the time at which the vortex structure breaks down, were based on near field plume measurements of NO and NO_2. A plume from a B747 was chased on 13 November 1994 during the POLINAT measurement campaign (Table 3). The measured parameter NO_c is used, and is defined as NO_c=NO+0.35NO_2. NO was measured by using the conventional NO/O_3 chemiluminescence technique. NO_2 was obtained by converting it photolytically to NO using broad band UV-light (320-420 nm) from a 500 W xenon arc lamp (Schlager et al., 1997). The reason for introducing NO_c is that the measurement technique only converts 35% of the sampled NO_2 to NO. The observed values of NO_c are plotted in Figure 3 versus plume age (upper panel) and versus vertical deviation from the mean track of the chased B747 (lower panel). During four (approximately equal) time periods extending between plume ages 85 to 87 s (number 1), 94 to 96 s (number 2), 100 to 107 s (number 3), and 123 to 126 s (number 4), the measured NO_c concentrations exceeded 5 ppbv. We assume that one of the trailing vortex pairs was penetrated during these periods.

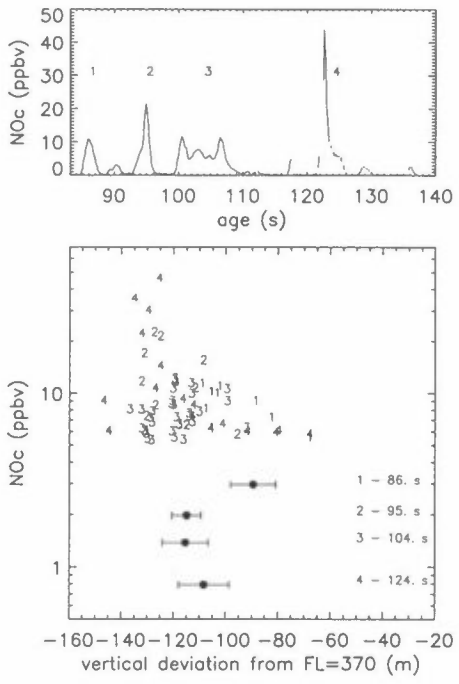

Figure 3: Upper panel: Measured NO_c values (NO_c=NO+0.35NO_2) versus plume age. The numbers denote four time periods during which one of the trailing vortex pairs was penetrated. Lower panel: The same NO_c data (>5 ppbv) plotted as numbers corresponding to the same four time periods versus vertical deviation from the flight level of the chased aircraft. The bold points and the bars (for which the vertical axis is without meaning) denote the mean position and the mean (Gaussian) vertical width of the vortex, respectively. The corresponding plume ages are also shown.

Now, let us consider the vertical displacements h_i from the flight level 370 hPa measured for the NO_c events during the considered periods. In each period, we denote their mean value with h_{vor} and their largest difference with d_{vor} and assign these quantities to the vertical vortex position and to the width of the vortex, respectively. The turbulence induced by the aircraft and by the atmosphere cause a meandering plume. Therefore we cannot assume that the vortex was centrally crossed during each time period. Consequently, the measured NO_c maximum, c_{max}, does not necessarily correspond to the NO_c values in the vortex core. We take this effect into account by using an appropriate Gaussian fit. One obtains $\sigma_{vor}^{exp} = d_{vor} / 2(\ln k)^{1/2}$ with $k = c_{max} / c_{limit}$, $c_{limit} = 5$ ppbv. The results for the absolute vortex positions (bold points), σ_{vor}^{exp} (bars) and corresponding plume ages are plotted in Figure 3. The absolute vortex positions indicate that the vortices are subject to a vertical displacement downward from the emission altitude. From the energy balance one can estimate the maximum vertical displacement of the trailing vortex pair at a given stratification N by $h_s = w_s/N$ where w_s is the initial downward velocity of the vortex pair. For the aircraft considered, w_s was estimated as 1.85 m s^{-1}. With N = 0.014 s^{-1} one obtains h_s = 132 m which agrees very well with the measured vertical displacements of the vortex pair (bold points in Figure 3. During the considered periods, the highest possible NO_c

concentrations were, probably not encountered. Consequently, the determined experimental values of σ_{vor}^{exp} give only an upper limit for the vortex width, and leads to $\sigma_{vor}(t = 124\ s) = 20$ m at the end of the vortex regime (see Figure 4).

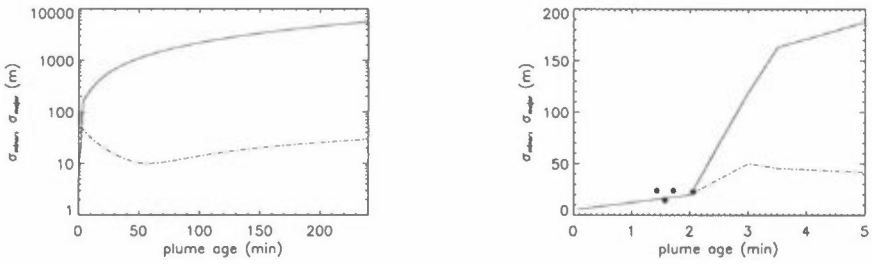

Figure 4: Temporal evolution of $\sigma_{major}(t)$ (solid line) and $\sigma_{minor}(t)$ (dot-dashed line). The bold points denote the values of σ_{vor} estimated from experimental data and correspond to the bars in Figure 3.

After $t = 124$ s the dispersion regime starts, characterised by sudden breaking of the vortex structure. Here, we assume that the diffusion regime is reached after $t = 3$ min with $\sigma_v = 50$ m and $\sigma_h = 120$ m (Schumann et al., 1995).

The diffusion coefficients for the diffusion regime are determined according to Dürbeck and Gerz (1995). For the given stratification $N = 0.014\ s^{-1}$ one obtains $D_v = 0.7\ m^2s^{-1}$ for $3 < t < 13$ min and $D_v = 0.15\ m^2s^{-1}$ for $3\ t > 13$ min, respectively. The horizontal diffusivity amounts to $D_h = 16.7\ m^2s^{-1}$. Additionally, relation $D_s = 0.5(D_vD_h)^{1/2}$ is assumed. The mean wind shear perpendicular to the mean plume direction amounts to $0.005\ s^{-1}$.

Making use of these parameters, an explicit description of the dispersion can be given in terms of $\sigma_{major}(t)$ and $\sigma_{minor}(t)$. The results are shown in Figure 4. Note, that despite the fact that σ_{minor} decreases during the plume dispersion, the effective cross section of the plume A (equation (9)) grows~($\sim t^2$).

3 Diffusion between the layers

The parameterisation of the mean diffusion between the layers is described in the following. The layers are divided into several sectors (Figure 5, marked area), and the concentration tendency due to diffusion for each sector is calculated. The mean concentration tendency in a plume layer for the chemical species is estimated by the equation

$$\frac{dc_{k,i}}{dt} = \frac{1}{V_i} \sum_{j=1,\ldots,n} \left(F_{i,j} - F_{i-1,j}\right) \qquad (13)$$

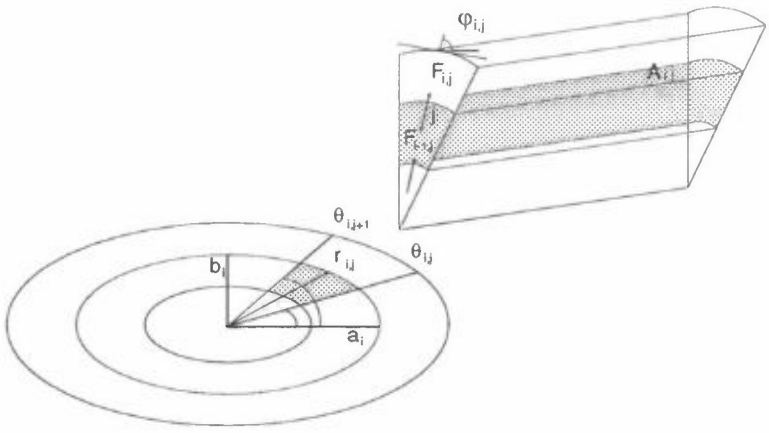

Figure 5: The plume is divided into several sectors. The marked area indicates the sector j *in a layer* i. *The marked sector is also shown from the side.*

where $c_{k,i}$ is the concentration of species k in layer i, the difference $F_{i,j} - F_{i-1,j}$ is the net diffusive influx of mass into layer i and sector j, $j = 1\ldots,n$ and V_i is the volume of each layer. The net diffusive influx through the boundary of a layer can be expressed as

$$F_{i,j} = K_j \frac{dc_{k,i}}{dr_{i,j}} A_{i,j}, \tag{14}$$

where K_j is the effective diffusion coefficient in the sector j, $r_{i,j}$ is the distance from the centre of the plume to the boundary of layer i for the angle $\frac{1}{2}(\theta_j + \theta_{j+1})$ and $A_{i,j}$ is the surface area of the sector j for the layer i (Figure 5. This area is estimated as

$$A_{i,j} = L \cdot r_{i,j}(\theta_{j+1} - \theta_j), \tag{15}$$

and

$$r_{i,j} = \left[\frac{b_i^2}{(1 - \varepsilon_i \cos^2 \theta_j)}\right]^{\frac{1}{2}}, \quad \varepsilon_i = \left[\frac{a_i^2 - b_i^2}{a_i}\right]^{\frac{1}{2}}, \tag{16}$$

where ε_i is the eccentricity of the ellipse in the ith layer.

K_j is calculated as a weighted sum of the diffusion coefficients in the direction of the major and minor principal axes. These coefficients are calculated for each layer by the equations (Csanady, 1973):

$$K_{major} = \frac{1}{2}\frac{d\sigma^2{}_{major}}{dt}, \quad K_{minor} = \frac{1}{2}\frac{d\sigma^2{}_{minor}}{dt}, \tag{17}$$

The parameterisation of $\sigma_{major}(t)$ and $\sigma_{minor}(t)$ during the vortex and dispersion regime was discussed in section 2. The effective diffusion coefficient K_j for a given sector is found based on the weighted sum of K_{major} and K_{minor}.

$$K_j = K_{major} \cos\varphi_{i,j} + K_{minor} \sin\varphi_{i,j} \tag{18}$$

Here, $\varphi_{i,j}$ is the angle between the gradient of the ellipse boundary at the point $(r_{i,j},(\theta_j + \theta_{j+1})/2)$ and the major axis (Figure 5. For an elliptic plume where the major axis is much greater than the minor, the mass flux in the plume has a larger component along the minor axis than along the major. With the weighting given in equation (18), $\varphi_{i,j}$ will approach 90° and the term including K_{minor} will dominate.

4 Chemistry

The photochemical module has been developed based on a boundary layer model (Hov et al., 1985), including a scheme describing both long and short-lived compounds. It has been modified to simulate free tropospheric conditions by including HNO_4, HNO_2 and some organic peroxides and organic nitrates. The module is well suited to study ozone chemistry, since it includes the precursors for ozone production and the formation of the hydroperoxyl radical (HO_2) and other peroxy radicals (RO_2) participating in the ozone production cycle. The following odd-nitrogen species (NO_y are included in the module:

$$\begin{aligned} NO_y \;=\; & NO + NO_2 + NO_3 + 2N_2O_5 + \\ & HNO_2 + HNO_3 + PAN + HNO_4 + \\ & CH_3NO_4 + CH_3ONO_2 + \\ & C_2H_5ONO_2 + C_4H_9ONO_2 \end{aligned} \tag{19}$$

The model is therefore a suitable tool for studying the conversion of NO_x ($NO+NO_2$) to less reactive nitrogen compounds like HNO_3, HNO_4, HNO_2, PAN and other organic nitrates.

The model calculates the concentrations of 66 chemical species. The quasi-steady-state-approximations (QSSA) method (Hesstvedt et al., 1978) including family grouping is used to estimate the time development of the chemical system. In the initial phase of the plume, the temporal development is rapid, and the time step has been set to 1 s. After 3 min, the temporal tendencies are smaller, and the time step is increased to 30 s.

Photo-dissociation rates have been precalculated, and values are established from look-up tables, using the function

$$J = Ae^{B\left(1.-1\frac{1.}{\cos(C\cdot\alpha)}\right)}, \tag{20}$$

where α is the solar zenith angle. The factors A, B and C are calculated for 17 reactions for 10 classes of 5 parameters. These parameters are the optical depth, cloud type and level, altitude, ground albedo, and total ozone column. Table 1 lists the classes used for the different parameters. The factors have been pre-calculated by Flatøy et al. (1995) based on a method developed by Isaksen et al. (1977) and Jonson and Isaksen (1991). The gasphase and photochemical reactions are listed in Table 2.

Table 1: The classes of total ozone column, cloud type and level, optical depth, altitude and ground albedo used to calculate the photo-dissociation rates.

Total ozone (DU)	Cloud type (bottom-top)	Optical depth	Height level (km)	Albedo
225	fog/clear: 0 - 1 km	0	1	0.1
250	convective: 1 - 3 km	1	2	0.2
275	convective: 1 - 4 km	2	3	0.3
300	convective: 1 - 6 km	4	4	0.4
325	convective: 1 - 8 km	8	5	0.5
350	stratiform: 2 - 4 km	16	6	0.6
375	stratiform: 4 - 6 km	32	7	0.7
400	stratiform: 6 - 8 km	64	8	0.8
425	stratiform: 9 - 10 km	128	9	0.9
450	stratiform: 12 - 13 km	256	10	1.0
			11	
			12	
			13	
			14	
			15	

Table 2: The tropospheric chemistry scheme used in the NILU-aircraft plume model. The numbers in brackets give the references used for the reaction rates: [1]:Atkinson et al. (1997), [2]:DeMore et al. (1997), [3]:Wayne et al. (1991), [4]:Atkinson et al. (1994), [5]:Atkinson et al. (1990), [6]: Peeters et al. (1993), [7]:Lightfoot et al. (1992), [8]:Bierbach et al. (1994), [9]:Wirtz et al (1994), [10]:DeMore et al. (1994), [11]:Atkinson et al. (1992) [12]:DeMore et al. (1992) [13]:Finlayson-Pitts and Pitts (1986)
Comments: ***n1****: Surface Pressure.,* ***n2****: Assumed to be 4.1x10^{-10}.* molec. cm^{-3}s^{-1}. *(Lattuati, 1997).,* ***n3****:* RNC_3H_6 *regroups β-peroxy nitrates which contain three or four carbons. OrgNitrates regroups β-oxy nitrates. Roxyl1 and* RNC_5H_8 *are the peroxy-nitrates from the degradation of 0-xylene and isoprene, respectively (Lattuati, 1997).,* ***n4****: Reaction rate assumed to be the same as reaction No. 66 (Lattuati, 1997),* ***n5****: Reaction rate assumed to be the same as reaction No. 62 (Lattuati, 1997).*

	Reaction	**Reaction rate**
1	$O(^3P) + O_2 + M \rightarrow O_3 + M$	$(6.0x10^{-34}[O_2]$ $+5.6x10^{-34}[N_2])x(T/300)^{-2.8}$ [1]
2	$O_3 + h\nu \rightarrow O^1(D) + O_2$	[2]
3	$O_3 + h\nu \rightarrow O^3(P) + O_2$	[2]
4	$O(^3P) + NO + M \rightarrow NO_2 + M$	$1.0x10^{-31}x(T/300)^{-1.6}N_2$ [1]
5	$O(^1D) + M \rightarrow O(^3P) + M$	$0.21x3.2x10^{-11}x10^{67./T}$ $+0.79x1.8x10^{-11}x10^{110/T}$ [1]
6	$O(^1D) + H_2O \rightarrow 2OH$	$2.2x10^{-10}$ [1]
7	$O_3 + NO \rightarrow NO_2 + O_2$	$1.8x10^{-12}exp(-1370/T)$ [1]
8	$O_3 + NO_2 \rightarrow NO_3 + O_2$	$1.2x^{-13}exp(-2450/T)$ [1]
9	$O_3 + OH \rightarrow HO_2 + O_2$	$1.9x10^{-12}exp(-1000/T)$ [1]
10	$O_3 + HO_2 \rightarrow OH + 2O_2$	$1.4x10^{-14}exp(-600/T)$ [1]
11	$NO_3 + NO \rightarrow 2NO_2$	$1.8x10^{-11}exp(110/T)$ [1]
12	$NO + HO_2 \rightarrow NO_2 + OH$	$3.7x10^{-12}exp(240/T)$ [1]
13	$2NO_3 \rightarrow 2NO_2 + O_2$	$8.5x10^{-13}exp(-2450/T)$ [2]
14	$NO_3 + H_2O_2 \rightarrow HO_2 + HNO_3$	$2.1x10^{(}-15)$ [12]
15	$NO_3 + h\nu \rightarrow NO + O_2$	[2]
16	$NO_3 + h\nu \rightarrow NO_2 + O$	[2]

Table 2, cont.

	Reaction	Reaction rate
17	$NO_2 + OH + M \rightarrow HNO_3 + M$	$k_0 = 2.6x10^{-30}(T/300)^{-2.9}N_2$ $k_\infty = 6.7x10^{-11}(T/300)^{-0.6}$ $F_c = 0.43$ [1]
18	$NO_2 + HO_2 + M \rightarrow HO_2NO_2 + M$	$k_0 = 1.8x10^{-31}x(T/300)^{-3.2}N_2$ $k_\infty = 4.7x10^{-12}$ $F_c = 0.6$ [1]
19	$HO_2NO_2 + M \rightarrow NO_2 + HO_2 + M$	$k_0 = 2.2x10^{-30}(T/300)^{-3.9}$ $k_\infty = 1.5x10^{-12}(T/300)^{-0.7}$ $Fc = 0.6$ [1]
20	$HO_2NO_2 + OH \rightarrow O_2 + O_2 + H_2O$	$1.5x10^{-12}exp(360./T)$ [1]
21	$HO_2NO_2 + h\nu \rightarrow HO_2 + NO_2$	[2]
22	$NO_2 + NO_3 \rightarrow NO + NO_2 + O_2$	$4.5x10^{-14}exp(-1260/T)$ [2]
23	$NO_2 + NO_3 + M \rightarrow N_2O_5 + M$	$k_0 = 2.7x10^{-30}(T/300)^{-3.4}N_2$ $k_\infty = 2.0x10^{-12}(T/300)^{0.2}$ $Fc = exp(-T/250)$ $+exp(-1059/T)$ [1]
24	$NO_2 + h\nu \rightarrow NO + O(^3P)$	[2]
25	$N_2O_5 + M \rightarrow NO_2 + NO_3 + M$	$k_0 = 1.03x10^{-3}(T/300)^{-3.5}x$ $exp(-11000/T)N_2$ $k_\infty = 9.7x10^{14}(T/300)^{0.1}x$ $exp(-11080/T)$ $Fc = exp(-T/250)$ $+exp(-1059/T)$ [1]
26	$N_2O_5 + H_2O \rightarrow 2HNO_3$	$2.0exp(-21)$ [1]
27	$N_2O_5 + h\nu \rightarrow NO_2 + NO_3$	[2]

Table 2, cont.

	Reaction	Reaction rate	
28	$OH + NO + M \rightarrow HONO + M$	$k_0 = 7.4x10^{-31}(T/300)^{-2.4}N_2$	
		$k_\infty = 4.5x10^{-11}$	
		$Fc = 0.9$	[1]
30	$OH + HONO \rightarrow NO_2 + H_2O$	$2.710x^{-12}x10^{260/T}$	[1]
31	$HONO + h\nu \rightarrow NO + OH$		[2]
32	$OH + H_2 + O_2 \rightarrow HO_2 + H_2O$	$7.7x10^{-12}exp(-2100/T)$	[1]
33	$OH + HO_2 \rightarrow H_2O + O_2$	$4.8x10^{-11}exp(250/T)$	[1]
34	$OH + H_2O_2 \rightarrow HO_2 + H_2O$	$2.9x10^{-12}exp(-160/T)$	[1]
35	$H_2O_2 + h\nu \rightarrow OH + OH$		[2]
36	$OH + HNO_3 \rightarrow NO_3 + H_2O$	$7.2x10^{-15}exp(785/T)$	
		$+1.9x10^{-33}exp(725/T)x$	
		$M/(1 + 1.9x10^{-33})xexp(725/T)$	
		$xM/(4.1x10^{-16}exp(1440/T))$	[1]
37	$HNO_3 + h\nu \rightarrow OH + NO_2$		[2]
38	$CO + OH(+O_2) \rightarrow HO_2 + CO_2$	$1.3x10^{-13}x(1 + 0.6\frac{P}{1000}(300/T))$	[1]
39	$HO_2 + HO_2 \rightarrow H_2O_2 + O_2$	$fH_20 * 2.2x10^{-13}exp(600./T)$	
	$fH_20 = 1. + 1.4x10^{-21}H_2Oexp(2200./T)$	$+fH_20x1.9x10^{-33}N_2exp(980./T)$	
40	$SO_2 + OH + M \rightarrow HO_2 + H_2SO_4$	$k_0 = 4.0x10^{-31}(T/300)^{-3.4}N_2$	
		$k_\infty = 2.0x10^{-12}$	
		$Fc = 0.45$	[1]
41	$SO_2 + CH_3O_2(H_2O + O_2) \rightarrow H_2SO_4 + HCHO + HO_2$	$2.0x10^{-21}$	[2]
	Methane chemistry		
42	$CH_4 + OH(+O_2) \rightarrow CH_3O_2 + H_2O$	$2.3x10^{-12}exp(-1765/T)$	[1]
43	$CH_4 + NO_3(+O_2) \rightarrow CH_3O_2 + HNO_3$	$4.0x10^{-19}$	[3]
44	$CH_3O_2 + NO(+O_2) \rightarrow HCHO + HO_2 + NO_2$	$4.2x10^{-12}exp(180/T)$	[1]

Table 2, cont.

	Reaction	Reaction rate
45	$CH_3O_2 + NO_2 + M \rightarrow CH_3NO_4 + M$	$k_0 = 2.5x10^{-30}(T/300)^{-5.5}N_2$ $k_\infty = 7.5x10^{-12}$ $Fc = 0.36$ [1]
46	$CH_3NO_4 + M \rightarrow CH_3O_2 + NO_2 + M$	$k_0 = 9.5x10^{-5}(-9690/T)N_2$ $k_\infty = 1.1x10^{16}exp(-10560/T)$ $Fc = 0.36$ [1]
47	$CH_3O_2NO_2 + h\nu \rightarrow CH_3O_2$	[2]
48	$CH_3O_2 + NO + M \rightarrow CH_3O_2NO + M$	0.005 k_{44} [4]
49	$CH_3NO_3 + OH(+O_2) \rightarrow HNO_3 + HCHO + HO_2$	$1.0x10^{-14}exp(1060/T)$ [4]
50	$CH_3NO_3 + h\nu \rightarrow HCHO + HONO$	[2]
51	$CH_3O_2 + HO_2 \rightarrow CH_3O_2H + O_2$	$3.8x10^{-13}exp(-780/T)$ [1]
52	$CH_3O_2H + OH \rightarrow 0.65[HCHO + OH + H_2O]$	$x2.9x10^{-12}exp(190/T)$ [1]
53	$CH_3O_2H + OH \rightarrow 0.35[CH_3O_2 + H_2O]$	$x2.9x10^{-12}exp(190/T)$ [1]
54	$CH_3O_2H + h\nu \rightarrow HCHO + HO_2 + OH$	[2]
55	$HCHO + OH(+O_2) \rightarrow CO + HO_2 + H_2O$	$8.6x10^{-12}exp(20/T)$ [1]
56	$HCHO + NO_3(+O_2) \rightarrow CO + HO_2 + HNO_3$	$5.8x10^{-16}$ [1]
57	$HCHO + 2HO_2 \rightarrow$ $0.4H_2O + 0.4HCOOH + 0.6HOCH_2OOH(+O_2)$	$2.14x10^{-41}exp(9925/T)$ [11]
58	$CH_2O + h\nu \rightarrow H + CHO$	[2]
59	$CH_2O + h\nu \rightarrow H_2 + CO$	[2]
	Ethane chemistry	
60	$C_2H_6 + OH(+O_2) \rightarrow C_2H_5O_2 + H_2O$	$7.9x10^{-12}exp(-1030/T)$ [1]
61	$C_2H_6 + NO_3(+O_2) \rightarrow C_2H_5O_2 + HNO_3$	$8.0x10^{-18}$ [3]
62	$C_2H_5O_2 + NO(+O_2) \rightarrow CH_3CHO + HO_2 + NO_2$	$8.7x10^{-12}$ [1]
63	$C_2H_5O_2 + NO + M \rightarrow C_2H_5ONO_2 + M$	0.014 k_{62} [4]
64	$C_2H_5ONO_2 + OH(+O_2) \rightarrow HNO_3 + CH_3CHO + HO_2$	$4.4x10^{-14}exp(1060/T)$ [4]

Table 2, cont.

	Reaction	Reaction rate
65	$C_2H_5ONO_2 + h\nu \rightarrow CH_3COO_2 + HONO$	[2]
66	$C_2H_5O_2 + HO_2 \rightarrow O_2 + C_2O_5H_2O$	$6.5x10^{-13}exp(650/T)$ [1]
67	$C_2H_5O_2H + OH \rightarrow 0.7C_2H_5O_2 + H_2O$	$2.7x10^{-12}exp(200/T)$ [10]
68	$C_2H_5O_2H + OH \rightarrow 0.3[CH_3CHO + OH + H_2O]$	$2.7x10^{-12}exp(200/T)$ [10]
69	$CH_3CHO + OH(+O_2) \rightarrow CH_3COO_2 + H_2O$	$5.6x10^{-12}exp(310/T)$ [1]
70	$CH_3CHO + NO_3(+O_2) \rightarrow CH_3COO_2 + HNO_3$	$1.4x10^{-12}exp(-1860/T)$ [1]
71	$CH_3CHO + h\nu \rightarrow CH_3O_2 + COHO2$	[13]
72	$CH_3COO_2 + HO_2 \rightarrow 0.67CH_3COO_2H$ $+0.67O_2 + 0.33CH_3COOH + 0.33O_3$	$4.3x10^{-13}exp(1040/T)$ [1]
73	$CH_3COO_2H + OH \rightarrow CH_3COO_2 + H_2O$	$2.7x10^{-12}exp(200/T)$ [10]
74	$CH_3COO_2 + NO_2 + M \rightarrow PAN + M$	$k_0 = 2.7x10^{-28} \cdot (T/300)^{-7.1} N_2$ $k_\infty = 1.2x10^{-11} \cdot (T/300)^{-0.9}$ $Fc = 0.3$ [1]
75	$PAN + M \rightarrow CH_3COO_2 + M + NO_2$	$k_0 = 4.9x10^{-3}exp(-12100/T)N_2$ $k_\infty = 5.4x10^{16}exp(-13830/T)$ $Fc = 0.3$ [1]
76	$PAN + OH + (O_2) \rightarrow NO_3 + HCOOH + CO_2 + H_2O$	$1.1x10^{-13}exp(-650/T)$ [4]
77	$PAN + h\nu \rightarrow CH_3COO_2 + NO_2$	[2]
78	$CH_3COO_2 + NO(+O_2) \rightarrow CH_3O_2 + NO_2 + CO_2$	$2.0x10^{-11}$ [1]
79	$C_2H_5OH + OH(+O_2) \rightarrow CH_3CHO + HO_2 + H_2O$	$4.1x10^{-12}exp(-70/T)$ [1]
80	$C_2H_5OH + NO_3 \rightarrow C_2H_5O_2 + HNO_3$	$9.0x10^{-16}$ [3]
	n- butane chemistry	
81	$nC_4H_{10} + OH(+O_2) \rightarrow secC_4H_9O_2 + H_2O$	$15x10^{-18}xT^2exp(190/T)$ [5]
82	$nC_4H_{10} + NO_3(+O_2) \rightarrow secC_4H_9O_2 + HNO_3$	$5.5x10^{-17}$ [3]
83	$secC_4H_9O_2 + NO \rightarrow 0.65CH_3COC_2H_5+$ $0.35CH_3CHO + 0.35C_2H_5O_2 + 0.65HO_2 + NO_2$	$4.0x10^{-12}$ [6]^{n2}

Table 2, cont.

	Reaction	Reaction rate
84	$CH_3COC_2H_5 + h\nu \rightarrow CH_3COO_2 + C_2H - 5O_2$	[13]
85	$secC_4H_9O_2 + NO + M \rightarrow C_4H_9ONO_2 + M$	$k_0 = 1.94x10^{-22}exp(4. \cdot 0.97)$ $k_\infty = 0.826(T/300)^{-8.1}$ $Fc = 0.411$ [4]^{n3}
86	$C_4H_9ONO_2 + OH(+O_2) \rightarrow RNC_3H_6 + H_2O$	$9.0x10^{-13}$ [4]
87	$C_4H_9ONO_2 + h\nu \rightarrow CH_3COC_2H_5 + HONO$	[2]
88	$secC_4H_9O_2 + HO_2 \rightarrow C_4H_9O_2H + HO_2$	$7.5x10^{-13}exp(700/T)$ [10]
89	$C_4H_9O_2H + OH(+O_2) \rightarrow 0.3[CH_3COC_2H_5 + OH + H_2O]$	$2.7x10^{-12}exp(200/T)$ [10]
90	$C_4H_9O_2H + OH(+O_2) \rightarrow 0.7[C_4H_9O_2 + H_2O]$	$2.7x10^{-12}exp(200/T)$ [10]
91	$CH_3COC_2H_5 + OH(+O_2) \rightarrow$ $CH_3COCH(O_2)CH_3 + H_2O$	$3.24x10^{-18}xT^2xexp(414/T)$ [4]
92	$CH_3COHCO + h\nu \rightarrow CH_3O_2 + CO + HO_2$	[2]
93	$CH_3COCHO_2CH_3 + NO(+O_2) \rightarrow$ $CH_3COCOCH_3 + HO_2 + NO_2$	$4.0x10^{-12}$ [6] ^{n2}
94	$CH_3COCOCH_3 + h\nu -> 2CH_3COO_2$	$0.036 \cdot J_{no2}$
95	$CH_3COCH(O_2)CH_3 + HO_2 \rightarrow CH_3COCH(O_2H)CH_3 + O_2$	$7.5x10^{-13}exp(700/T)$ [10]^{n4}
	ethene chemistry	
96	$C_2H_4 + OH(+O_2) \rightarrow CH_2(O_2)CH_2OH + M$	$k_0 = 7.9x10^{-29} \cdot (T/300)^{-3.1}N_2$ $k_\infty = 9.10x10^{-8.1}$ $Fc = 0.7$ [1]
97	$C_2H_4 + O_3 \rightarrow 2HO_2 + CO$	$9.1x10^{-15}exp(-2580/T)$ [1]
98	$C_2H_4 + NO_3(+O_2) \rightarrow CH_2(O_2)CH_2ONO_2 + O_2$	$2.0x10^{-16}$ [3]
99	$CH_2(O_2)CH_2OH + NO(+O_2) \rightarrow 2.HCHO + HO_2 + NO_2$	$8.7x10^{-12}$ [10]^{n3,n5}
100	$CH_2(O_2)CH_2OH + HO_2 \rightarrow HO_2CH_2CH_2OH + O_2$	$7.5x10^{-13}exp(700/T)$ [10]^{n4}
101	$CH_2(O_2)CH_2ONO_2 + NO(+O_2) \rightarrow OrgNitrate + NO_2$	$8.7x10^{-12}$ [10]^{n4}
	propene chemistry	

Table 2, cont.

	Reaction	Reaction rate	
102	$C_3H_6 + OH(+O_2) \rightarrow CH_3CHO_2CH_2OH + M$	$k_0 = 8.0x10^{-27} \cdot (T/300)^{-3.5} N_2$ $k_\infty = 3.0x10^{-11}$ $Fc = 0.5$	[1]
103	$C_3H_6 + O_3 \rightarrow 0.50CH_3CHO + 0.40CO + 0.31CH_3O_2 +$ $0.30HCHO + 0.09CH_3COOH + 0.15OH + 0.065CH_4$ $+0.07H_2 + 0.22H_2O + 0.325 + CO_20.185HCOOH + 0.28HO_2$	$5.5x10^{-15}exp(1880/T)$	[1]
104	$C_3H_6 + NO_3(+O_2) \rightarrow RNC_3H_6$	$9.45x10^{-15}$	[3][n3]
105	$CH_3CH(O_2)CH_2OH + NO(+O_2) \rightarrow$ $CH_3CHO + HCHO + HO_2 + NO_2$	$4.0x10^{-12}$	[6] [n2]
106	$CH_3CH(O_2)CH_2OH + HO_2 \rightarrow$ $CH_3CH(O_2H)CH_2OH$	$7.5x10^{-13}exp(650/T)$	[10][n4]
107	$RNC_3H_6 + NO \rightarrow OrgNitrate + NO_2$	$4.0x10^{-12}$	[6] [n2,n3]
	oxylene chemistry		
108	$oxylene + OH(+2O_2) \rightarrow oxyl1$	$13.7x10^{-12}$	[5]
109	$oxylene + NO_3(+2O_2) \rightarrow roxyl1$	$3.7x10^{-16}$	[3][n3]
110	$oxyl1 + NO(+2O_2) \rightarrow CH_3COCHO + HO_2$ $+CH_3COCH = CHCHO + NO_2$	$4.0x10^{-12}$	[6][n2]
111	$oxyl1 + HO_2 \rightarrow oxylh1 + H_2O$	$7.5x10^{-13}exp(650/T)$	[2][n4]
112	$CH_3COCH = CHCHO + OH(+O_2) \rightarrow$ $CH_3COCHOHCHO_2CHO$	$5.6x10^{-11}$	[8]
113	$CH_3COCH(OH)CH(O_2)CHO + NO(+O_2) \rightarrow$ $CH_3COCHO + HCOCHO + HO_2 + NO_2$	$4.0x10^{-12}$	[6][n2]
114	$CHOCHO + h\nu \rightarrow HCHO + CO$		[2]
115	$roxyl1 + NO \rightarrow OrgNitrate + NO_2$	$4.0x10^{-12}$	[6][n2,n3]
	Isoprene chemistry		
116	$C_5H_8 + OH(+O_2) \rightarrow HOC_5H_8O_2$	$25.4x10^{-12}exp(410/T)$	[9]

Table 2, cont.

	Reaction	Reaction rate	
117	$C_5H_8 + NO_3 \rightarrow RNC_5H_8$	$7.8x10^{-13}$	[9][n3]
118	$HOC_5H_8O_2 + NO \rightarrow CH_3COCHCH_2 + HO_2 + HCHO + NO_2$	$1.4x10^{-11}exp(180/T)$	[9]
119	$HOC_5H_8O_2 + HO_2 \rightarrow perox$	$7.5x10^{-13}exp(700/T)$	[10][n4]
120	$CH_3COCH = CH_2 + OH(+O_2) \rightarrow CH_3COCH(OH)CH_2O_2$	$4.1x10^{-12}exp(453/T)$	[9]
121	$NO + CH_3OHCOCHCH_2O_2(+O_2) \rightarrow$ $MGLYOx + HCHO + HO_2 + NO_2$	$1.4x10^{-11}exp(180/T)$	[9][n3]
122	$RNC_5H_8 + NO \rightarrow OrgNitrate + HO_2$	$1.4x10^{-11}exp(-180/T)$	[9]
	RO_2 + RO_2 reactions		
123	$2CH_3O_2(+O_2) \rightarrow A[2.HCHO + 2.HO_2]$	$1.1ex10^{-13}exp(365/T)$	[1]
124	$2CH_3O_2(+O_2) \rightarrow (1-A)[CH_3OH + HCHO]$	$1.1ex10^{-13}exp(365/T)$	[1]
	$A = 25.exp(-1165/T)(1 + 25.exp(-1165/T)$		[7]
125	$2C_2H_5O_2 + O_2 \rightarrow B[2.CH_3CHO + 2.HO_2]$	$9.8x10^{-12}exp(-100/T)$	[1]
126	$2C_2H_5O_2 + O_2 \rightarrow (1-B) \quad [CH_3CHO + C_2H_5OH]$	$9.8x10^{-12}exp(-100/T)$	[1]
	$B = 10.2exp(-533/T)/(1. + 10.2exp(-533/T)$		[7]
127	$2CH_3COO_2O_2 \rightarrow 2.CH_3O_2 + CO_2$	$2.8x10^{-12}exp(530/T)$	[1]
	RO_2 + R'O_2 reactions		
128	$CH_3COO_2 + CH_3O_2(+O_2) \rightarrow \sqrt{C}[HCHO + CH_3O_2 + HO_2 + CO_2]$	$5.1 \cdot 10^{-12}exp(272/T)$	[1]
129	$CH_3COO_2 + CH_3O_2(+O_2) \rightarrow \sqrt{(1-C)}[HCHO + CH_3COOH]$	$5.1 \cdot 10^{-12}exp(272/T)$	[1]
	$C = 4.4 \cdot 10^5 exp(-3910/T)/(1 + 4.4 \cdot 10^5 exp(-3910/T))$		[7]
130	$C_2H_5O_2 + CH_3O_2(+O_2) \rightarrow a1[CH_3CHO + HCHO + 2HO_2]$	$(2\sqrt{k_{123}k_{125}})$	[7]
131	$C_2H_5O_2 + CH_3O_2(+O_2) \rightarrow a3[CH_3CHO + CH_3OH]$	$2\sqrt{k_{123}k_{125}}$	[7]
132	$C_2H_5O_2 + CH_3O_2(+O_2) \rightarrow 2[C_2H_5OH + HCHO]$	$2\sqrt{k_{123}k_{125}}$	[7]
	$a1 = \sqrt{AB}$		[7]
	$a2 = (1-A)(1-a1)/(2-A-B)$		[7]
	$a3 = (1-B)(1-a1)/(2-A-B)$		[7]

Table 2, cont.

Reaction	Reaction rate
133 $C_2H_5O_2 + CH_3COO_2(+O_2) \rightarrow$	
$\sqrt{B}[CH_3CHO + HO_2 + CH_3O_2 + CO_2]$	$2\sqrt{k_{127}k_{125}}$ [7]
134 $C_2H_5O_2 + CH_3COO_2(+O_2) \rightarrow$	
$(1-\sqrt{B})[CH_3CHO + CH_3COOH]$	$2\sqrt{k_{127}k_{125}}$ [7]
135 $C_4H_9O_2 + CH_3O_2(+O_2) \rightarrow a4[0.65CH_3COC_2H_5$	
$+(1-0.65)CH_3CHO + (1-0.65)C_2H_5O_2$	
$+0.65HO_2 + HCHO + HO_2]$	$2\sqrt{k_{123}1.7x10^{-12}exp(-2188/T)}$ [7]
136 $C_4H_9O_2 + CH_3O_2(+O_2) \rightarrow a5[0.65CH_3COC_2H_5$	
$+(1-0.65)CH_3CHO + (1-0.65)C_2H_5O_2 + CH_3OH]$	$2\sqrt{k_{123}1.7x10^{-12}exp(-2188/T)}$ [7]
137 $C_4H_9O_2 + CH_3O_2(+O_2) \rightarrow a6[0.65CH_3COC_2H_5$	
$+(1-0.65)CH_3CHO + (1-0.65)C_2H_5O_2 + HCHO]$	$2\sqrt{k_{123}1.7x10^{-12}exp(-2188/T)}$ [7]
138 $C_4H_9O_2 + CH_3COO_2(+O_2) \rightarrow \sqrt{D}[0.65CH_3COC_2H_5$	
$+(1-0.64)CH_3CHO + (1-0.65)C_2H_5O_2$	
$+0.65HO_2 + CH_3O_2 + CO_2]$	$2\sqrt{k_{123}1.9x10^{-13}exp(745/T)}$ [7]
$a4 = \sqrt{DA}$	[7]
$a5 = (1-D)(1-\sqrt{AD})/(2-A-D)$	[7]
$a6 = (1-A)(1-\sqrt{AD})/(2-A-D)$	[7]
$D = 50exp(-1165/T)/(1+50exp(-1165/T)$	[7]
139 $C_4H_9O_2 + CH_3COO_2(+O_2) \rightarrow (1-\sqrt{D})[0.65CH_3COC_2H_5$	
$+(1-0.65)CH_3CHO + (1-0.65)C_2H_5O_2 + CH_3COOH]$	$2\sqrt{k_{123}1.9x10^{-13}exp(745/T)}$ [7]
140 $CH_2(O_2)CH_2OH + CH_3O_2(+O_2) \rightarrow$	
$A[2HCHO + HCHO + 2HO_2]$	$2\sqrt{k_{127}1.9x10^{-13}exp(745/T)}$ [7]
141 $CH_2(O_2)CH_2OH + CH_3O_2(+O_2) \rightarrow$	
$(1-A)/2[2HCHO + CH_3OH]$	$2\sqrt{k_{127}1.9x10^{-13}exp(745/T)}$ [7]
142 $CH_2(O_2)CH_2OH + CH_3O_2(+O_2) \rightarrow$	
$(1-A)/2[2HCHO + HCHO]$	$2\sqrt{k_{127}1.9x10^{-13}exp(745/T)}$ [7]

Table 2, cont.

Reaction	Reaction rate	
143 $CH_2(O_2)CH_2OH + CH_3COO_2(+O_2) \rightarrow$		
$\sqrt{A}[2HCHO + HO_2 + CH_3O_2 + CO_2]$	$2\sqrt{k_{127}1.9x10^{-13}exp(745/T)}$	[7]
144 $CH_2(O_2)CH_2OH + CH_3COO_2(+O_2) \rightarrow$		
$(1 - \sqrt{A})[CH_3CHO + CH_3COOH]$	$2\sqrt{k_{127}1.9x10^{-13}exp(745/T)}$	[7]
145 $CH_3COCH(O_2)CH_3 + CH_3O_2(+O_2) \rightarrow$		
$a4[CH_3COCOCH_3 + HCHO + 2HO_2]$	$2\sqrt{k_{123}1.2x10^{-13}}$	[7]
146 $CH_3COCH(O_2)CH_3 + CH_3O_2(+O_2) \rightarrow$		
$a5[CH_3COCOCH_3 + CH_3OH]$	$2\sqrt{k_{123}1.2x10^{-13}}$	[7]
147 $CH_3COCH(O_2)CH_3 + CH_3O_2(+O_2) \rightarrow$		
$a6[CH_3COCOCH_3 + HCHO]$	$2\sqrt{k_{123}1.2x10^{-13}}$	[7]
148 $CH_3COCH(O_2)CH_3 + CH_3COO_2(+O_2) \rightarrow$		
$\sqrt{D}[CH_3COCOCH_3 + HO_2 + CH_3O_2 + CO_2]$	$2\sqrt{k_{127}1.2x10^{-13}}$	[7]
149 $CH_3COCH(O_2)CH_3 + CH_3COO_2(+O_2) \rightarrow$		
$+(1 - \sqrt{D}[CH_3COCCH_3 + CH_3COOH]$	$2\sqrt{k_{127}1.2x10^{-13}}$	[7]
150 $CH_3CH(O_2)CH_2OH + CH_3O_2(+O_2) \rightarrow$		
$a4[CH_3CHO + 2HCHO + 2HO_2]$	$2\sqrt{k_{123}3.5x10^{-14}}$	[7]
151 $CH_3CH(O_2)CH_2OH + CH_3O_2(+O_2) \rightarrow$		
$+a5[CH_3CHO + HCHO + CH_3OH]$	$2\sqrt{k_{123}3.5x10^{-14}}$	[7]
152 $CH_3CH(O_2)CH_2OH + CH_3O_2(+O_2) \rightarrow$		
$a6[CH_3CHO + 2HCHO]$	$2\sqrt{k_{123}3.5x10^{-14}}$	[7]
153 $CH_3CH(O_2)CH_2OH + CH_3COO_2(+O_2) \rightarrow$		
$\sqrt{D}[CH_3CHO + HCHO + HO_2 + CH_3O_2 + CO_2]$	$2\sqrt{k_{127}3.5x10^{-14}}$	[7]
154 $CH_3CH(O_2)CH_2OH + CH_3COO_2(+O_2) \rightarrow$		
$+(1 - \sqrt{D}[CH_3CHO + HCHO + CH_3COOH]$	$2\sqrt{k_{127}3.5x10^{-14}}$	[7]
155 $C_8H_{10}OH = O_2 + CH_3O_2(+O_2) \rightarrow$		
$a4[CH_3COCHO + CH_3COCH - CHCHO + HCHO + 2HO_2]$	$2\sqrt{k_{123}1.2x10^{-13}}$	[7]

Table 2, cont.

	Reaction	**Reaction rate**	
156	$C_8H_{10}OH - O_2 + CH_3O_2(+O_2) \rightarrow$ $a5[CH_3COCHO + CH_3COCH = CHCHO + CH_3OH]$	$2\sqrt{k_{123}1.2x10^{-13}}$	[7]
157	$C_8H_{10}OH = O_2 + CH_3O_2(+O_2) \rightarrow$ $a6[CH_3COCHO + CH_3COCH = CHCHO + HCHO]$	$2\sqrt{k_{123}1.2x10^{-13}}$	[7]
158	$C_8H_{10}OH - O_2 + CH_3COO_2(+O_2) \rightarrow \sqrt{D}[CH_3COCHO+$ $CH_3COCH = CHCHO + HO_2 + CH_3O_2 + CO_2]$	$2\sqrt{k_{127}1.2x10^{-13}}$	[7]
159	$C_8H_{10}OH - O_2 + CH_3COO_2(+O_2) \rightarrow (1 - \sqrt{D})[CH_3COCHO$ $+CH_3COCH = CHCHO + CH_3COOH]$	$2\sqrt{k_{127}1.2x10^{-13}}$	[7]
160	$CH_3COCH(OH)CH(O_2)CHO + CH_3O_2(+O_2) \rightarrow$ $a4[CH_3COCHO + HCOCHO + HCHO + 2HO_2]$	$2\sqrt{k_{123}3.8x10^{-14}}$	[7]
161	$CH_3COCH(OH)CH(O_2)CHO + CH_3O_2(+O_2) \rightarrow$ $a5[CH_3COCHO + HCOCHO + CH_3OH]$	$2\sqrt{k_{123}3.8x10^{-14}}$	[7]
162	$CH_3COCH(OH)CH(O_2)CHO + CH_3O_2(+O_2) \rightarrow$ $a6[CH_3COCHO + HCOCHO + HCHO]$	$2\sqrt{k_{123}3.8x10^{-14}}$	[7]
163	$CH_3COCH(OH)CH(O_2)CHO + CH_3COO_2(+O_2) \rightarrow$ $\sqrt{D}[CH_3COCHO + HCOCHO + HO_2 + CH_3O_2 + CO_2]$	$2\sqrt{k_{127}3.8x10^{-14}}$	[7]
164	$CH_3COCH(OH)CH(O_2)CHO + CH_3COO_2(+O_2) \rightarrow$ $(1 - \sqrt{D})[CH_3COCHO + HCOCHO + CH_3COOH$	$2\sqrt{k_{127}3.8x10^{-14}}$	[7]
165	$OHC_5H_8O_2 + CH_3O_2(+O_2) \rightarrow a4[0.3CH_2 = C(CH_3)CHO$ $+O_3CH_3COCH = CH_2 + 1,6HOHo + 2HO_2]$	$2\sqrt{k_{123}3.8x10^{-14}}$	[7]
166	$OHC_5H_8O_2 + CH_3O_2(+O_2) \rightarrow a5[0,3CH_2 - C(CH_3)CHO$ $+0.3CH_3COCH = CH_2 + 0,6HCHO + CH_3OH]$	$2\sqrt{k_{123}3.8x10^{-14}}$	[7]
167	$OHC_5H_8O_2 + CH_3O_2(+O_2) \rightarrow 6[0.3CH_2 = C(CH_3)CHO$ $+0.3CH_3COCH - CH_2 + 1,6HCHO]$	$2\sqrt{k_{123}3.8x10^{-14}}$	[7]
168	$OHC_5H_8O_2 + CH_3COO_2(+O_2) \rightarrow \sqrt{D}[0.3CH_2 = C(CH_3)CHO$ $+0.3CH_3COCH = CH_2 + 0.6HCHO + 0,6HO_2 + CH_3O_2 + CO_2]$	$2\sqrt{k_{127}3.8x10^{-14}}$	[7]

Table 2, cont.

	Reaction	Reaction rate	
169	$OHC_5H_8O_2 + CH_3COO_2(+O_2) \rightarrow$		
	$(1-\sqrt{D})[0.3CH_2=C(CH_3)CHO$		
	$+0.3CH_3COCH=CH_2+0.6HCHO+CH_3COOH]$	$2\sqrt{k_{127}3.8x10^{-14}}$	[7]
170	$CH_3COCH(OH)CH_2O_2 + CH_3O_2(+O_2) \rightarrow$		
	$a4[CH_3COCHO+2HCHO+2HO_2]$	$2\sqrt{k_{123}3.8x10^{-14}}$	[7]
171	$CH_3COCH(OH)CH_2O_2 + CH_3O_2(+O_2) \rightarrow$		
	$+a5[CH_3COCHO+HCHO+CH_3OH]$	$2\sqrt{k_{123}3.8x10^{-14}}$	[7]
172	$CH_3COCH(OH)CH_2O_2 + CH_3O_2(+O_2) \rightarrow$		
	$+a6[CH_3COCHO+2HCHO]$	$2\sqrt{k_{127}3.8x10^{-14}}$	[7]
173	$CH_3COCH(OH)CH_2O_2 + CH_3COO_2(+O_2) \rightarrow$		
	$\sqrt{D}[CH_3COCHO+HCHO+HO_2+CH_3O_2+CO_2]$	$2\sqrt{k_{127}3.8x10^{-14}}$	[7]
174	$CH_3COCH(OH)CH_2O_2 + CH_3COO_2(+O_2) \rightarrow$		
	$+(1-\sqrt{D})[CH_3COCHO+HCHO+CH_3COOH]$	$2\sqrt{k_{127}3.8x10^{-14}}$	[7]

5 Experimental setup

An example of aircraft emissions from a B747 are listed in Table 3. The emissions are calculated as g kg^{-1}, which in this case gives an NO_x emission rate of 37.05 g s^{-1}. At the start of the vortex regime, the horizontal and vertical standard deviation of the plume is set equal 6 m (section 2). The horizontal and vertical radius of the plume is set to $3 \cdot \sigma_h$ and $3 \cdot \sigma_v$, respectively. The emissions are homogeneously distributed within the 6 inner layers of the plume, while the 2 outer layers rapidly will be influence by emissions due to diffusion within the plume. The distribution of the hydrocarbon emissions is based on suggestions from Pleijel et al., (1993), and is listed in Table 4.

Since we start the calculations at the beginning of the vortex regime, some of the emitted NO_x is already converted to reservoir species. The amount converted is dependent on the NO_x and OH emitted at the engine exit. Based on Kärcher et~al., 1996 (Figure 10a, 10b and 12) we assume that 1.5% of the emitted NO was converted to HNO_2, 4% of the emitted NO_2 was converted to HNO_3 and that 2.3% of an OH value of 6.2 ppmv at the engine exit was converted to H_2O_2.

Table 3: Emissions of the considered B747. True air speed is the speed relative to the wind speed. The given emission indices The value of $EI[NO_x]=12.5\ g\ kg^{-1}$ was based on near field plume measurements (Schulte et al., 1997).

Parameter	Units	Value
Engine type		CF6-80C2B1F
True Air Speed *V*	[m s^{-1}, Ma]	247.0, 0.84
EI[H_2O]	[g kg^{-1}]	1242.0
EI[CO_2]	[g kg^{-1}]	3153.0
EI[SO_2]	[g kg^{-1}]	1.0
EI[CO]	[g kg^{-1}]	1.5
EI[NO_x]	[g kg^{-1}]	12.5
EI[HC]	[g kg^{-1}]	0.2
Fuel consumption	[kg km^{-1}]	12.0

Table 4: Specification of the hydrocarbon emission based on suggestions from Pleijel et al. (1993).

Species	Vol. Frac.~(%)	Mass Frac.~(%)
Alkanes:		
methane	34.83	17.87
ethane	0.19	0.18
butane	9.58	17.82
Alkenes:		
ethene	23.56	21.16
propene	5.67	7.68
Aromatics:		
o-xylene	1.32	4.49
Oxygenates:		
formaldehyde	14.08	13.55
acetaldehyde	7.29	10.29
glyoxal	2.41	4.48
methylglyoxal	1.08	2.49

The formation and evolution of particles are prescribed in the aircraft plume model. The particle evolution is calculated with a model which is developed to analytically describe the nucleation of an aerosol driven by the condensation of condensable vapour (Ford, 1996). The calculations performed here, use an initial soot aerosol with a number density of 2.4×10^6 cm^{-3} at the engine exit, taking the form of a lognormal size distribution with a mean radius of 30 nm and a geometric standard deviation of two. Figure 6 shows two examples of the particle evolution in the plume when the temperature was 214 K and the relative humidity was 42% and 62%, respectively. (Only results after 10 s of simulations are shown.) In the first case, the air was not supersaturated with respect to ice. At

about 0.1 seconds into the simulation, the particles are activated, which is to say that a large amount of water condenses on to the particles. The aerosol melts after an activated period of about 10 seconds, and stabilises at a radius of about 0.09 µm with a highly acidic composition. The soot particles were assumed to be coated with a layer of H_2SO_4/H_2O (Kärcher, 1997). In the second case, ice particles started to grow in the plume. The number and radius of the particles formed in the plume were used to calculate the surface area density of particles.

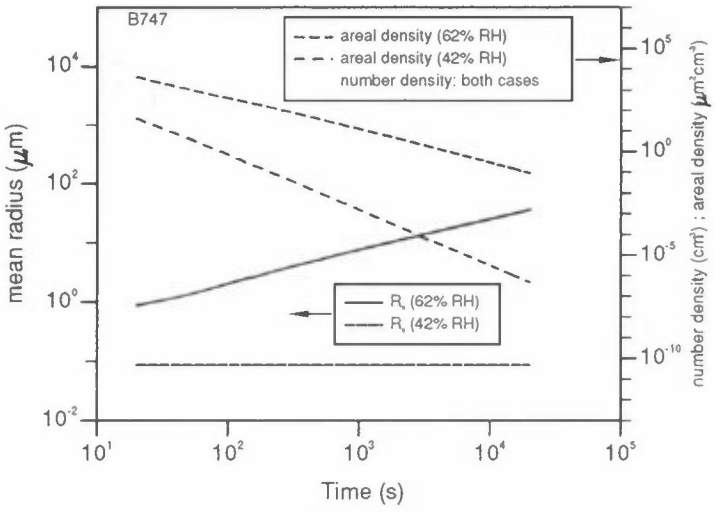

Figure 6: Evolution of mean radius, number density and area density for soot-based aerosol, for two cases with 42% and 62% ambient relative humidity.

The reaction rates for heterogeneous reactions are calculated as

$$k = \frac{\gamma \cdot A \cdot c}{4}, \tag{21}$$

where γ is the reactive uptake coefficient, A is the particle surface area density and c is the molecular velocity. In the tropospheric version of the plume model the following heterogeneous reaction was included;

$$N_2O_5 + H_2O \rightarrow 2HNO_3 \tag{22}$$

The uptake coefficient for sulphate aerosols recommended by DeMore et al. (1997) was used for coated soot. When ice particles form, the uptake coefficient recommended for so called PSC type 2 particles was used. These particles consist of a core of NAT (nitric acid trihydrate), and an outer layer of ice. Since the heterogeneous reactions on PSC 2 particles are surface reactions, it seems reasonable to use these uptake coefficients for heterogeneous reactions on ice particles in the plume.

6 Acknowledgements

This work was funded by the European Commission under contract number EV5V-CT93-0310, the Research Council of Norway and the Norwegian Civil Aviation Administration. The authors would like to thank Inga Fløisand, Sverre Solberg and Frode Flatøy for comments and dicussion of the manuscript.

7 References

Atkinson, R., Baulch, D.L., Cox, R.A., Hampson Jr., R.F., Kerr, J.A., Rossi, M.J. and Troe, J. (1997) Evaluated kinetic, Photochemical and Heterogeneous Data for Atmospheric Chemistry. Supplement V, IUPAC Subcommittee on Gas Kinetic Data Evaluation for Atmospheric Chemistry. *J. Phys. and Chem. Ref Data, 26*, 521-1011.

Atkinson, R., Baulch, D.L., Cox, R.A., Hampson Jr., R.F., Kerr, J.A., Rossi, M.J. and Troe, J. (1994) Gas-phase tropospheric chemistry of organic compounds. *J. Phys. and Chem. Ref Data*, Monograph n°2.

Atkinson, R., Baulch, D.L., Cox, R.A., Hampson Jr., R.F., Kerr, J.A. and Troe, J. (1992) Evaluated kinetic and Photochemical Data for Atmospheric Chemistry. Supplement IV, IUPAC Subcommittee on Gas Kinetic Data Evaluation for Atmospheric Chemistry. *Atmos. Environ., 26A,* 1167-1230.

Atkinson, R. (1990) Gas-phase tropospheric chemistry of organic compounds: A review. *Atmos. Environ., 24A,* 1-41.

Bierbach, A., Barnes, I., Becker, K.H. and Wiesen, E. (1994) Atmospheric Chemistry of Unsaturated Carbonyl: Butendial, 4~Oxo-2-pentenal, 3-Hexen-2,5-dione, Maleic Anhydride, 3H-Furan-2-one and 5-Methyl-3H-furan-2-one, to be published in Environment Science Science Technologie, LACTOZ re-evaluation of the EMEP MSC-W photo oxidant model. *EUROTRAC, Lactoz.*

Csanady, G.T. (1973) Turbulent Diffusion in the Environment. Dordrecht, Reidel (Geophysics and Astrophysics Monographs, 3D).

DeMore, W.B., Sander, S.P., Goldes, D.M., Molina, M.J., Hampson, R.F., Kurylo, M.J., Howard, C.J., Ravishankara, A.R. and Kolb, C.E. (1997) Chemical kinetics and photochemical data for use in stratospheric modeling. Evaluation number 12. Pasadena, Jet Propulsion Lab. (JPL Publication 97-4).

DeMore, W.B., Sander, S.P., Goldes, D.M., Molina, M.J., Hampson, R.F., Kurylo, M.J., Howard, C.J., Ravishankara, A.R. and Kolb, C.E. (1994) Chemical kinetics and photochemical data for use in stratospheric modeling. Evaluation number 11. Pasadena, Jet Propulsion Lab. (JPL Publication 94-26).

DeMore, W.B., Sander, S.P., Goldes, D.M., Molina, M.J., Hampson, R.F., Kurylo, M.J., Howard, C.J., Ravishankara, A.R. and Kolb, C.E. (1992) Chemical kinetics and photochemical data for use in stratospheric modeling. Evaluation number 10. Pasadena, Jet Propulsion Lab. (JPL Publication 92-20).

Dürbeck, T. and Gerz, T. (1995) Large-eddy simulation of aircraft exhaust plumes in the free atmosphere: Effective diffusivities and cross-sections. *Geophys. Res. Lett., 22*, 3203-3206.

Finlayson-Pitts, B and Pitts, J.N. (1986) Atmospheric Chemistry: Fundamentals and Experimental Techniques. New York, Wiley, pp. 182.

Flatøy, F., Hov, Ø. and Smit, H. (1995) 3-D model studies of vertical exchange processes in the troposphere over Europe. *J. Geophys. Res., 6*, 11,465-11,481.

Ford, I.J., Hayman, G.D. and Kingdon, R.D. (1996) Plume and aerosol modelling for the Polinat project: Final report: *Pollution from Aircraft emissions in the North Atlantic Flight Corridor (Polinat),* (ed. U. Schumann). Report EUR 16978, European Commission, 258-279.

Fløisand, I. and Stordal, F. (1999) Modelling of heterogeneous chemistry in the stratosphere. Kjeller (NILU OR 11/98) (under arbeid).

Grønskei, K. E., Walker, S. E. and Gram, F. (1993) Evaluation of a model for hourly spatial concentration distributions. *Atmos. Environ., 27B*, 105-120.

Hesstvedt, E., Hov, Ø. and Isaksen, I.S.A. (1978) Quasi-steady-state approximations in air pollution modelling. Comparison of two numerical schemes of oxidant prediction. *Int. J. Chem. Kinet., 10*, 971-994.

Hoshizaki, H., Anderson, L. B., Conti, R.J., Farlow, N., Meyer, J.W., Overcamp, T., Redler, K.O. and Watson, V. (1975) Aircraft wave microscale phenomena. In: *The stratosphere perturbed by propulsion effluents. Chapter 2.*

Hov, Ø., Stordal, F, and Eliassen, A. (1985) Photochemical oxidant control strategies in Europe: A 19 days case study using a Lagrangian model with chemistry. Lillestrøm (NILU TR 5/85).

Isaksen, I.S.A., Midtbø, K.H., Sunde, J., and Crutzen, P.J. (1977) A simplified method to include molecular scattering and reflection in calculation of photo fluxes and photo dissociation rates. *Geophys. Norv., 31*, 11-26.

Jonson, J.E. and Isaksen, I.S.A. (1991) The impact of solar flux variations on the tropospheric ozone chemistry. Oslo, Institute of Geophysics, University of Oslo (Institute report series/Institutt for geofysikk, Universitetet i Oslo, nr. 81).

Kärcher, B. (1997) Heterogeneous chemistry in aircraft wakes: Constraints for uptake coefficients. *J. Geophys. Res., 102*, 19,119-19,135.

Kärcher, B., Hirschberger, M.~M. and Fabian, P. (1996) Small-scale chemical evolution of aircraft exhaust species at cruising altitudes. *J. Geophys. Res., 101*, 15,169-15,190.

Kärcher, B. (1995) A trajectory box model for aircraft exhaust plumes. *J. Geophys. Res., 100*, 18,835-18,844.

Konopka, P. (1995) Analytical Gaussian solutions for anisotropic diffusion in a linear shear flow. *J. Non-Equilib. Thermodyn., 20*, 78-91.

Kraabøl, A.G., Konopka, P., Stordal, F., Ford, I. and Fløisand, I. (1999) Particles and heterogeneous chemistry in aircraft plumes. Pollution from aircraft emissions in the North Atlantic Flight Corridor (POLINAT 2). Report EUR 18877, edited by U. Schumann, 289-306.

Kraabøl, A.G., Konopka, P., Stordal, F. and Knudsen, S. (1997) Turbulent mixing and chemistry in the aircraft wake. Pollution from aircraft emissions in the North Atlantic Flight Corridor (POLINAT). Report EUR 16978, edited by U. Schumann, 234-257.

Lattuati, M. (1997) Contribution à l'étide du bilan de l'ozone tropospérique à l'interface de l'Europe et de l'Atlantique nord: modélisation lagrangienne et mesures en altitude. Ph.D. Thesis, 239.

Lightfoot, P.D., Cox, R.A., Crowley, J.N., Destriau, M., Haymann, G.D., Jenkin, E., Moortgart, G.K. and Zabel, F. (1992) Organic peroxy radicals: kinetics, spectroscopy and tropospheric chemistry. *Atmos. Environ., 26A*, 1805-1961.

Peeters, J. et al. (1993) Rate constants of the reactions of CF3O2, iC3H7O2, tC4H9O2 and sC4H9O2 with NO. In: Proceedings of EUROTRAC Symposium. Ed. by P M. Borell et al., The Hague.

Pleijel, K., Moldanovä, J. and Andersson-Sköld, Y. (1993) Chemical modelling of an aeroplane exhaust plume in the free troposphere. Göteborg, IVL (IVL Report B; 1105).

Schumann, U., Konopka, P., Baumann, R., Busen, R., Gerz, T., Schlager, H., Schulte, P. and Volkert, H. (1995) Estimation of diffusion parameters of aircraft exhaust plumes near the tropopause from nitric oxide and turbulence measurements. *J. Geophys. Res., 100*, 14,147-14,162.

Schlager, H., Konopka, P. Schulte, P., Schumann, U., Ziereis, H., Arnold, F., Klemm, M., Hagen, D., Whitefield, P. and Ovalez, J. (1997) In situ Observations of Aircraft Emissions Signatures in the North Atlantic Flight Corridor. *J. Geophys. Res., 102*, 10,739-10,750.

Schulte, P., Schlager, H., Ziereis, H. and Schumann, U. (1997) NO_x emission indices of subsonic lon-range aircraft at cruise altitude: In situ measurements and predications. *J. Geophys. Res., 102*, 21,431-21,442.

Wayne, R.P., Barnes, I., Biggs, P., Burrows, J.P., Canosa-Mas, C.E., Hjorth, J., Le Bras, G., Moortgat, G.K., Perner, D., Poulet, G., Restelli, G. and Sidebottom, H. (1991) The nitrate radical: Physics, chemistry, and the atmosphere. *Atmos. Environ., 25*, 1-203.

Wirtz, K. Roehl, C., Hayman, G.D., Jenkin, M.E. (1994) LACTOZ Re-evaluation of the EMEP MSC-W Photooxidant model. Garmisch-Partenkirchen, EUROTRAC.

Norwegian Institute for Air Research (NILU)
P.O. Box 100, N-2027 Kjeller, Norway

REPORT SERIES	REPORT NO. TR 4/99	ISBN 82-425-1098-9	
TECHNICAL REPORT		ISSN 0807-7185	
DATE 6.8.99	SIGN.	NO. OF PAGES 30	PRICE NOK 45,-

TITLE

The NILU aircraft plume model:
A technical description

PROJECT LEADER

Anne Gunn Kraabøl

NILU PROJECT NO.

E-99091

AUTHOR(S)

Anne Gunn Kraabøl, Frode Stordal,
Paul Konopka and Svein Knudsen

CLASSIFICATION *

A

CONTRACT REF.

REPORT PREPARED FOR
Norwegian Institute for Air Research (NILU)
P.O. Box 100, N-2027 Kjeller, Norway

ABSTRACT

The NILU-aircraft plume model combines the chemical and physical evolution in an aircraft plume. It describes the plume within a day after emissions. This report gives a detailed description of the plume dispersion, the diffusion within the different layers of the plume and the tropospheric chemistry scheme used in the model.

NORWEGIAN TITLE

NILUs fly-plume modell: En teknisk beskrivelse

KEYWORDS		
Aircraft plume	Gaussian dispersion	Tropospheric chemistry

ABSTRACT (in Norwegian)

En plume-modell som beskriver kjemisk og fysisk utvikling av eksosen fra fly er utviklet. Denne rapporten gir en detaljert beskrivelse av plume-spredningen, diffusjonen i plumen og det kjemiske skjemaet som er inkludert i modellen.

* *Classification*
- *A Unclassified (can be ordered from NILU)*
- *B Restricted distribution*
- *C Classified (not to be distributed)*